URN (Paper): urn:nbn:de:gbv:ilm1-2014iwk-155:2

58th ILMENAU SCIENTIFIC COLLOQUIUM
Technische Universität Ilmenau, 08 – 12 September 2014
URN: urn:nbn:de:gbv:ilm1-2014iwk:3

Hammering beneath the surface of Mars – Modeling and simulation of the impact-driven locomotion of the HP^3-Mole by coupling enhanced multi-body dynamics and discrete element method

Roy Lichtenheldt[1], *Bernd Schäfer*[2], *Olaf Krömer*[3]

[1] German Aerospace Center (DLR), Institute of System Dynamics and Control
[1] Ilmenau University of Technology, Department of Mechanical Engineering, Mechanism Technology Group
[2] German Aerospace Center (DLR), Institute of Robotics and Mechatronics
[3]German Aerospace Center (DLR), Institute of Space Systems

ABSTRACT

As the formation of the rocky planets in our inner solar system has always been a major subject of scientific interest, NASA's discovery mission InSight (Interior Seismic Investigations, Geodesy and Heat Transport) intends to gain further knowledge about the interior structure of Mars. In order to understand the processes that lead to planetary evolution, Mars' seismic as well as thermal properties will be measured. DLR's HP^3-Mole (Heat Flow and Physical Properties Package), an innovative self impelling nail, will hammer itself into the red planet deeper than any other instrument before, in order to measure the heat flux and thermal gradient down to a final depth of 5 m. To achieve this challenging goal, high fidelity simulation models have been used throughout the whole development process. To meet the demands on accuracy, two detailed models were created based on enhanced multi-body dynamics and discrete element techniques. For the most detailed analysis both methods are coupled to enable further understanding of the interaction between Mole mechanism and soil dynamics. Validation has been carried out for every existing prototype stage of the mechanism and has shown very good correlation between measurement and simulation. Additionally the soil model is compared to penetration tests in real soil as well as cone penetrometer measurements. Using these simulation models various influences can be evaluated by virtual prototypes in the actual environmental conditions of Mars, which would not be achieved in reality before the start of the mission. By supporting the design with detailed simulations, it was possible to increase the locomotion performance while reducing the consumed power remarkably, i.e. by less than 5 W of input power.

Index Terms - discrete element method, multi-body simulation, co-simulation, planetary exploration, Mole, virtual prototyping, terramechanics

1. INTRODUCTION

In order to further investigate the formation and evolution of terrestrial planets in our inner solar system, NASA's mission InSight (Interior Seismic Investigations, Geodesy and Heat Transport) aims to analyze seismic and thermal properties of Mars [1]. Therefore DLR's HP^3-Instrument (Heat Flow and Physical Properties Package) will measure Mars' interior heat flux and thermal gradient down to a depth of 5 m and thus deeper below the Martian surface than any other instrument before. Being the locomotion system of the instrument, the HP^3-Mole is working as a

self impelling nail in order to accomplish this goal. The inner hammering mechanism is spring driven and periodically loaded by a cylindrical cam mechanism. The innovative impact driven locomotion principle enables a minimum in required energy and mass, but leads to complex system behaviour and dependence of the inner mechanism dynamics on the outer force conditions exerted by the soil.
In order to understand the mechanism's dynamic behaviour as well as to investigate influencing parameters for the support of the mission related design process of the HP^3-Mole, numerical models in several levels of detail have been set up. One core part of these modular models is the multi-body model of the hammering mechanism, covering the inner dynamics including the contact driven energy transmission. In an early stage of development [2] this model has been used to analyze the basic mechanism behaviour and the parameter influences, by attaching it to an elasto-plastic soil interaction model. Furthermore in [2] the model has been used to perform a multi-objective optimization, in order to determine an optimal set of design parameters as well as further parameter influences. Therefore a special optimization process is used and the optimization is carried out using the framework MOPS (Multi-Objective Parameter Synthesis), originally presented in [3]. In [4] the model is successfully applied to forensic engineering of observed actuator failures.
The actual environmental conditions of Mars will not be achieved in reality before the start of the mission. Hence the simulation models are used to evaluate the design in the actual Martian conditions. Therefore the multi-body models presented in [2] and [4] need to be adapted in order to cover new effects of the flight design as well as to be fully independent of preliminary parameter calibration by measurements. To meet these demands a new approach to model the inner gas flow of the Mole based on dynamic pneumatic networks has been developed and is explained in this paper.
Even though most of the mechanism optimization results were used in the flight model of the HP^3-Mole, there is still optimization potential left regarding the outer shape. First analysis for investigation of the tip's influence by simulation has been carried out by [5] for a similar system. In order to further understand the influence of the outer shape, a soil model based on the discrete element method proposed for planetary rovers in [6], is used in this paper to analyze the interaction and to prepare the investigation of additional influences. In order maintain the overburden pressure in a certain depth while limiting the number of particles to a minimum, an enhanced dynamic simulation domain boundary approach is presented. As the mechanism's dynamic behaviour is highly dependent on the interaction with the soil, a co-simulation approach, coupling multi-body simulations (MBS) and discrete element method is further developed and validated. Moreover a sequential process is developed in order to efficiently prepare the co-simulations. Since the interaction between the Mole and the soil is still not fully understood, this approach enables further insight to the microscale origins of macroscale effects. Hence the developed approach and the gained knowledge will help to develop and optimize future Mole systems.

2. HP^3-MOLE: SETUP & OPERATIONAL PRINCIPLE

The HP^3-Mole is divided in two main parts: The hammering mechanism for locomotion purpose and the payload compartment containing the scientific payload STATIL. As obstacles like stones will deflect the Mole's trajectory, STATIL is used to determine the Mole's inclination during the penetration phase. Thus together with the TLM (Tether Length Measurement), the absolute depth of the Mole can be determined. As the impact driven locomotion principle causes a high shock environment, STATIL (Static Tilt measurement unit) needs to be suspended by two galaxy shaped shock isolation springs. Additionally the outer hull is equipped with the payload

TEM-A (Thermal Excitation Measurement-Active) to measure the heat flux below the Martian surface. On the Mole's back, the science tether, equipped with the TEM-P (Thermal Excitation Measurement-Passive) temperature sensors, is mounted in order measure the annular temperature wave of Mars and to supply the Mole with electric energy.
The hammering mechanism consists of three main masses: Hammer, suppressor and outer hull. The suppressor is containing most of the tensioning mechanism's parts, which is periodically

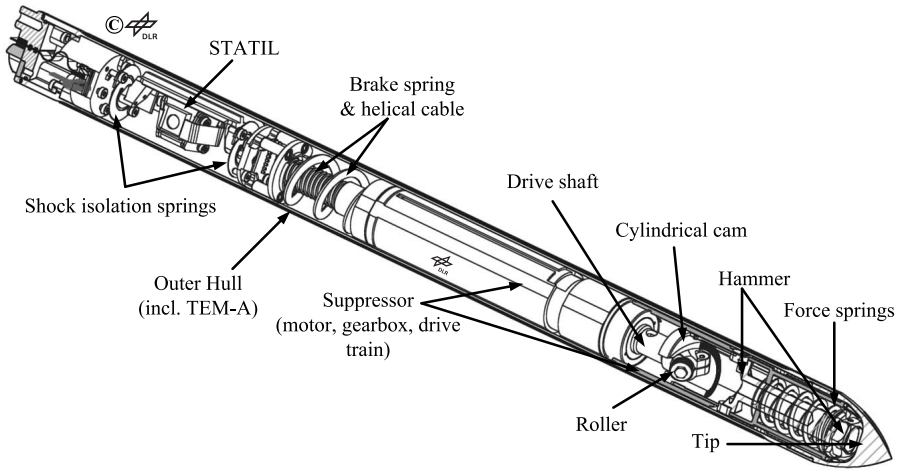

Figure 1: Cut through the HP^3-Mole

loading the force springs. The hammer is containing a cylindrical cam, which is used to load the force springs.
Due to the results in [2] and the needed design adaptions in [4], the current design changed dramatically compared to former prototypes investigated in [2] and [4]. Figure 1 shows a cut through the current setup of the Mole. Despite many design related improvements and inclusion of the optimization results, an additional change with significant impact on dynamics is the ability of the hammer to separate from the force springs. Thus the hammer is given more time to transmit the energy to the outer hull and consequently the efficiency of the mechanism shall be improved.
Nevertheless the main operational principle of the Mole is preserved: The inner hammering mechanism is driven periodically by two force springs. In order to load the force springs the Mole is actuated by a DC-motor unit, continuously driving a cylindrical cam mechanism. The hammer is pulled away from the tip by this tensioning mechanism while loading the force springs. After reaching the maximum spring deflection, the hammer is released due to a gap in the cylindrical cam. Thereafter the complex operational cycle of the stroke process takes place. When the cylindrical cam mechanism is releasing the force springs, the hammer is accelerated towards the tip by the springs. The suppressor is suspended by the brake spring in order suppress parasitic upwards motion of the hull. Thus the suppressor is accelerated upwards as well. Since the suppressor mass is chosen several times higher [2] than the hammer mass, most of the spring energy is transformed to the hammer's kinetic energy. When the force springs are totally relaxed again, the hammer is supposed to separate from the springs and move freely before it actually impacts the tip (referred to as first stroke). After the suppressor met its point of reversal, the suppressor mass moves towards the tip again, driven by gravity and the brake spring. Finally as a consequence of the mechanism's operation principle, the suppressor impacts the tip (referred to as second stroke) and causes additional penetrating motion of the outer hull. Due to rebounds of the parts subsequent strokes occur, but are supposed to be irrelevant for the locomotion. Hence this second stroke can be used beneficially to increase the achieved penetration depth, but is also able to cause damage to the actuator if parameters are not properly

chosen. The subsequent strokes occur either until the system is at rest or until the tensioning starts anew. The inner operation is not observable even in case of using transparent casings, as the mechanism is subject to high speed operation, high shock loads and the operation inside the soil. In order to better understand the operational principle, and moreover, to gain further knowledge about the mechanisms behaviour, multi-body dynamics models as well as particle based soil models were developed and adapted to analyze and improve the HP^3-Mole. Thus further details on the operational cycle are given in a later section as the mechanism is analyzed using the numerical models.

3. MODELING & SIMULATION

As the inner operation of the mechanism is not visually observable due to high shock loads and operation in soil simulants, numerical models are used to analyze the dynamic behaviour. Thus a multi-body dynamics model has been developed in [2] and was further adapted due to the demands of the mission [4]. To cover the mechanisms behaviour on Mars, in this paper final

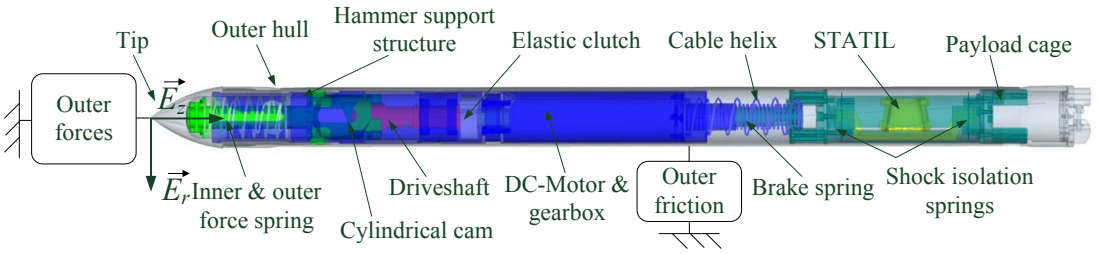

Figure 2: Overview of the HP^3-Mole multi-body model

adaptions are carried out and the multi-body model is coupled to the discrete element models described in [6]. An overview of the modular multi-body model is shown in Figure 2. The main features of the multi-body models are:

- bodies and their kinematical relationship,
- tensioning and release mechanism including the DC-motor in the electro-dynamic domain,
- contact dynamics,
- force and brake springs,
- environmental conditions for Mars and Earth,
- critical body surface friction effects inside the Mole,
- internal gas flow based on dynamic pneumatic networks,
- influence of the spring suspended payload STATIL, used to estimate the Mole's inclination,
- modular external force conditions (Health Check Test Stand (HCTS), elasto-plastic soil, discrete element soil a.o.).

The discrete element (DE) models have originally been developed to model wheels of planetary exploration rovers driving in soft sandy soil. The main features of these DE soil models are (cf. [6], [7]):

- efficient adaption of anisotropic particle rotation by usage of 2D-rotation geometries,
- efficient computation of nonlinear cohesion effects on grain level,
- dynamic boundaries of the simulation domain,
- bulk density dependent on gravity,
- apriori determination strategy of the micro parameters by macroscopic measurements,
- modeling toolchain implemented in an individual framework.

As a special demand due to the usage in planetary exploration, the models need to be able to predict the dynamic behaviour of the instrument under terrestrial as well as Martian environmental conditions. Lacking the opportunity to test directly under Martian conditions (i.e. on Mars) before launch, the models are virtual prototypes operated in the actual environment. Therefore the models need to be validated using terrestrial conditions and hence to have the potential to reliably predict the driving dynamics under Martian conditions afterwards. This requires a model dependent only on measurable macroscopic parameters, as parameter calibration by on-site measurements is no option. In order to use different outer force conditions, the multi-body model is designed in a modular way. Thus it can be used with a variety of outer force modules like the HCTS, empirical soil model used in [2] to optimize the mechanism, discrete element soil models etc. The dynamic models including their main important features are described in detail throughout the next sections.

3.1. Enhanced Multi-body & Contact Modeling of the Hammering Mechanism

The impact driven locomotion principle and the high number of (partially) free moving or spring suspended bodies result in complex dynamic behaviour of the mechanism. In order to keep results interpretable the multi-body models of the Mole are existing in several levels of detail. This enables the use of models which are as complex as needed, but as simple as possible. Throughout this section only the highest level of detail models are explained.

To lower the mechanism's complexity in simulation, the parts are clustered into higher-level bodies. The individual parts of those bodies are assumed to have no relative motion with respect to other parts of the same body. Thus most bolted and threaded joints, as well as glued and welded bonds are treated as perfect connections. Furthermore all bodies are assumed to be perfectly rigid. Local deformations due to the impacts are covered by the respective contact dynamics laws. Springs are modeled as ideal elastic elements. Hence they are modeled massless, linear and of finite length. The latter two points are accounted for by assigning correspondent piecewise linear force-displacement relations, in order to allow the attached bodies to separate from the spring if needed. In addition to the actual brake spring the cable guiding helix as well as the attached cables are modeled as elastic elements.

Using this approach, a maximum number of nine moving bodies is achieved. Those bodies are interacting by several force laws accounting for the inner effects in the mechanism. The most important bodies for the stroke cycle analysis are shown in Figure 2: The hammer (green), the suppressor (blue) consisting of motor, gearbox, motor housing and hammer support structure and the outer hull (grey) consisting of the tip, payload cage, backcap, TEM-A, the outer hull assembly itself and smaller subassemblies. Dissipation takes place due to stick-slip friction forces between the individual bodies. The respective friction coefficients are determined by the material interfaces, lubrication and expected normal pressure. The corresponding normal forces are either calculated online wherever possible or are assumed to create a worst case. Dependent

on the scenario and aim of the simulation, such worst case can be highest as well as lowest expected friction. Additional dissipation is implicitly added due to the motion induced gas flow inside the mechanism, contact laws, as well as the DC-motor model.
The inner contact dynamics are covered by applying HERTZian contact as shown in [2] to cover the elastic deformation during the impact. By adding linear damping in order to model the dissipation during the impact, the general contact force formulation is derived as

$$\vec{F}_{\mathrm{C}} = \left(\frac{2E}{3(1-\nu^2)} \sqrt{r_{\mathrm{C}} \delta^3} + k\dot{\delta} \right) \vec{e}_z \tag{1}$$

where δ is the contact deflection and $\dot{\delta}$ the relative velocity while the contact is active respectively. Furthermore E is YOUNG's Modulus, ν POISSON's ratio, k the contact damping coefficient and r_{C} the equivalent contact radius. Thereby r_{C} is chosen dependent on the geometry of the respective contact interface. As described in [2], contacts are grouped as functional and possible contacts. For the group of functional contacts, YOUNG's Modulus and POISSON's ratio are chosen as the correspondent materials values and combined to a value for the contact interface. The contact damping k is determined by the coefficient of restitution of the contact interface, as well as the critical damping. According to [8], the damping coefficient derives to:

$$k = 2 \frac{\ln(\epsilon_{\mathrm{r}})}{\sqrt{\ln(\epsilon_{\mathrm{r}})^2 + \pi^2}} \cdot \sqrt{c_{\mathrm{eq}} m} \tag{2}$$

where ϵ_{r} is the coefficient of restitution, c_{eq} is the equivalent stiffness and m the equivalent mass respectively.
During the tensioning process the interaction between the drive shaft's roller and the cylindrical cam needs to be covered. According to [2] using a soft contact approach leads to ineffective models as well as errors in the achieved force spring load and energy. As the force spring's load is increasing, a soft contact approach would lead to growing overlaps and thus increasing errors during the tensioning process. The highest errors would arise when the roller is situated at the cam's edge M_{ed} (Fig.3 left). As this influences the release process, the cam mechanism itself is modeled analytically by mathematical constraint equations. For the modeling procedure, the three dimensional representation (Fig.3 right) is projected into cylindrical coordinates as a two dimensional slope (Fig.3 left). In the two dimensional representation, θ denotes the non-constant slope angle and F_z, F_γ are the forces in $\vec{e}_z$ and $\vec{e}_\gamma$ direction, respectively. Furthermore γ is the rotation angle of the drive shaft and μ the sticking friction coefficient of the roller-cam interface. The constraint between roller and slope profile is modeled by $z\left(\gamma(t)\right)$, which

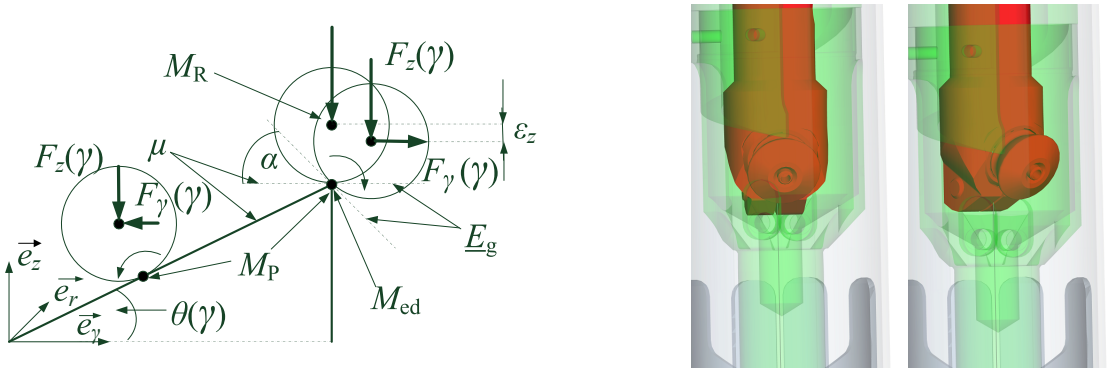

Figure 3: Principle of the tensioning process model in cylindrical coordinates (cf.[4]) (left) and 3D animation of the tensioning/release process on the nonlinear cam (right)

is the slope profile with respect to the roller's center of rotation M_{R}. Thus the resulting torque is derived using an adapted form of the correspondent equation presented in [2] covering the optimized nonlinear cam profile:

$$\vec{M}_{\mathrm{K}} = \left(\frac{z'\left(\gamma(t)\right) + \mu_{\mathrm{r}}}{1 - z'\left(\gamma(t)\right) \cdot \mu_{\mathrm{r}}} \sum_{j=1}^{n} c_{1j} \cdot z\left(\gamma(t)\right) \right) \cdot \vec{e}_{\gamma} \times r_{\mathrm{K}} \cdot \vec{e}_{r} \tag{3}$$

whereby r_{K} is the equivalent radius of the cylindrical cam in $\vec{e}_r$ direction and μ_{r} is the coefficient of rolling friction between the roller and the cam surface.
After reaching the highest elevation of the cam profile the roller rotates further, while its instantaneous center of rotation remains on M_{ed}. The tangential force F_{γ}, pointing in negative direction of $\vec{e}_{\gamma}$ while loading the spring, is exerted by the spring force F_z and the cam's slope. By crossing the top of the cam, F_{γ} changes sign and is then acting in positive direction of $\vec{e}_{\gamma}$. The equivalent friction plane $\underline{\mathbf{E}}_{\mathrm{g}}$ is defined perpendicular to $\overline{M_{\mathrm{P}} M_{\mathrm{R}}}$ and thus its angle α can be used to check the sticking state at M_{P}. If $F_{\gamma} \times r_{\mathrm{K}}$ is not sufficiently high to accelerate the drive shaft around $\vec{e}_z$, the roller stays in contact at M_{P} until the sticking friction is exceeded by the resultant force in the $\vec{e}_z \vec{e}_{\gamma}$ plane. As this static release process will lead to a loss of preload length ε_z and thus available force spring energy, a dynamic release process is intended in order to achieve the condition $\varepsilon_z \to 0$. To cover this dynamic release process, forces are only applied if $M_{\mathrm{P}} \in z(\gamma)$ is satisfied.
In order to support the dynamic release process even at higher friction, the drive shaft is connected to the gearbox by means of an elastic clutch, featuring a defined maximum deformation angle. This clutch is loaded during the tensioning process and relaxes during the release process. Thus in addition to $F_{\gamma} \times r_{\mathrm{K}}$ the elastic torque accelerates the drive shaft in $\vec{e}_z$ direction and hence the roller is "thrown" off the cam. As the older prototypes of the Mole used a non-elastic version of the clutch, an adaption of the torque equation with respect to [2] and [4] is applied. Thus the clutch torque $\vec{M}_{\mathrm{C}}$ is defined as:

$$\vec{M}_{\mathrm{C}} = \vec{e}_z \begin{cases} -c_{\gamma} \Delta\gamma & ; \forall \Delta\gamma \leq 0 \\ c_{\mathrm{c}} \Delta\gamma & ; \forall \Delta\gamma \in (0, \gamma_0) \\ c_{\gamma} \Delta\gamma & ; \forall \Delta\gamma \geq \gamma_0 \end{cases} \tag{4}$$

where c_{c} is the stiffness of the elastic part of the clutch and c_{γ} is the contact stiffness. Thereby the condition $c_{\mathrm{c}} << c_{\gamma}$ has to be fullfilled. Moreover $\Delta\gamma$ is the difference of the rotation angles between gearbox and drive shaft with the rotation range of the clutch γ_0.
In order to cover effects like the load drop and corresponding speed up of the voltage driven brushed DC-motor during the release process, the electro-dynamics of the motor have been integrated into the dynamic system model by applying KIRCHHOFF's and NEWTON's laws (cf. [10]):

$$U_{\mathrm{A}} = R_{\mathrm{A}} I_{\mathrm{A}}(t) + L_{\mathrm{A}} \dot{I}_{\mathrm{A}}(t) + k_U \dot{\gamma}_{\mathrm{A}}(t) \tag{5}$$

$$J_{\mathrm{A}} \ddot{\gamma}_{\mathrm{A}}(t) = k_M I_{\mathrm{A}}(t) - k_{\mathrm{d}} \dot{\gamma}_{\mathrm{A}}(t) - c_{\mathrm{A}} \Delta\gamma_{\mathrm{A}}(t) - M_{\mathrm{i}} \cdot \operatorname{sign}\left(\dot{\gamma}_{\mathrm{A}}(t)\right) - \sum M_{\mathrm{L}}(t) \tag{6}$$

In these coupled differential equations R_{A}, L_{A}, I_{A} and U_{A} are the rotor terminal resistance, inductance, current and voltage, respectively. Torsional stiffness c_{A} and angular deflection $\Delta\gamma_{\mathrm{A}}$ are accounting for twisting deformation in the rotor shaft. J_{A} and k_{d} are the rotor's moment of inertia and damping coefficient, respectively. Moreover k_M is the motor's torque constant, k_U the mutual induction constant and M_{i} the static friction torque. The mechanical part of the

model exerts the load torques M_L via the planetary gearbox. This gearbox is modeled by its gear ratio, inertia and an equivalent rotational stiffness.
The interaction of the bodies with the forces caused by internal gas flows are modeled as a dynamic pneumatic network. The setup of this network is shown in Figure 4. Thereby q_h and q_s denote the hammer's and the suppressor's position respectively. It consists of three main

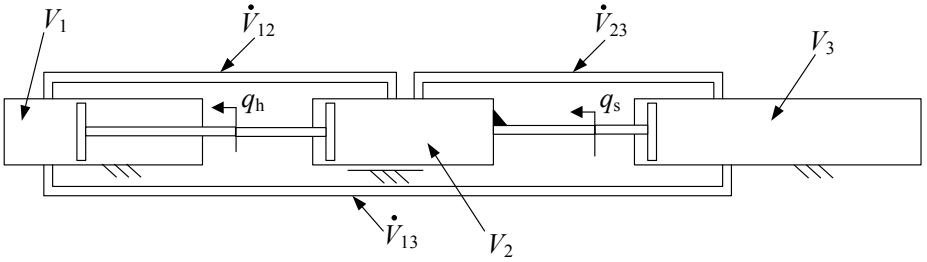

Figure 4: Pneumatic network used to model the internal gas flow

volumes, which are dependent on the bodies' positions. These volumes are interconnected by pipes in order to cover the gas flow around the mechanism's parts. The pipes are assumed to have a circular cross section, equal to the cross section of the dedicated flow paths of the suppressor, hammer and hammer support structure. As the change in position of the bodies changes the volumes and thus changes the pressures each time step, the flow is instationary and based on BERNOULLI's equation. Hence the acceleration of the pipe volume can be acquired as (cf. [9]):

$$\ddot{V}_{ij} = \frac{1}{l_{ij}\rho}\left(A_{ij}\left(p_i - p_j\right) - \frac{\rho}{2A_{ij}}\dot{V}_{ij}^2 - \dot{V}_{ij}^2 \cdot \mathrm{sign}(\dot{V}_{ij}) \cdot \frac{\rho}{2A_{ij}}(\kappa_\mathrm{F}\frac{l_{ij}}{d_{ij}} + \zeta)\right) \tag{7}$$

$$\dot{V}_{ij} = A_{ij}w \tag{8}$$

with w the mean velocity in the pipe flow. Furthermore V_{ij}, A_{ij}, l_{ij} and d_{ij} are the transported volume, cross sectional area, length and diameter of the pipe between chamber i and j respectively. The dissipation takes place by pipe friction κ_F and drag ζ. The density of the medium ρ is dependent on the ambient pressure p_0 on the planetary body, the ambient temperature T_0 as well as the special gas constant R_s:

$$\rho = \frac{p_0}{R_s T_0} \tag{9}$$

with the correspondent values supplied by mission related documents. The chamber's volume V_i is calculated from its initial volume at the previous time step, the actual length of the chamber and the volume fed through the pipe connection by the pressure difference at the previous time step. By updating the length of the chamber by the actual body positions, the volume derives to:

$$V_i(t+\delta t) = V_i(t) + A_i \cdot (l_i - q_i(t)) + \sum_j V_{ij}(t) \tag{10}$$

with A_i being the projected face area of the moving bodies, l_i the initial length of the chamber and q_i the actual position of the moving bodies relative to the initial length. Assuming an isothermal state change, pressure p_i in each chamber is derived from its volume V_i before and after the step. Using this pressure the gas force acting on the corresponding body is calculated by:

$$F_i(t+\delta t) = A_i p_i(t)\frac{V_i(t)}{V_i(t+\delta t)} \tag{11}$$

As the model is based only on geometric as well as environmental parameters, it is suitable to cover the conditions on Earth as well as on Mars.

3.2. Particle-based Terramechanics

In [2] a simple empirical soil model featuring an elasto-plastic element is used in order to keep the simulation time short enough to enable multi-objective optimization of the mechanism. The model is covering the qualitative effects of the interaction with the soil and was originally calibrated by measurements taken from PINNA et al. [11]. However they are not capable to cover the actual soil deformation field and effects of the outer shape. In order to get further detailed results on the soil interaction and deformation as well as the influences of the outer shape, particle-based methods are applied.

The Discrete Element Method (DEM) has first been announced by CUNDALL & STRACK [12] in 1979. It is based on the discretisation of the simulation domain by distinct particles, interacting by contact forces and torques. As DEM is a meshfree method, the particles are free to move

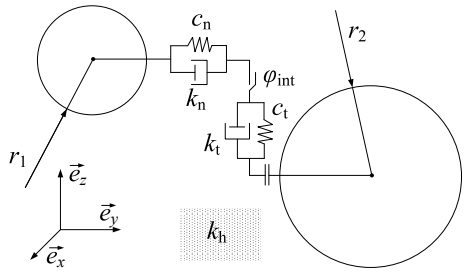

Figure 5: Particle interaction model in normal and tangential direction of the contact [6]

and contact each other in 6DOF without fixed neighboring relations. Even though the method itself would be able to cover each grain by one particle, nowadays hardware still lacks the computational power. Thus in the DLR-SR "**D**iscrete **E**lement **M**ethod **E**nabled **T**e**r**ramechanics **I**nteraction fr**a**mework" (DEMETRIA) based on the particle simulation tool Pasimodo [13], particles are treated as pure discretisation objects and suitable assumptions and approximations are applied in order to scale the particles' size.

In order to obtain the normal forces between interacting particles a similar soft contact approach as shown in Eq.1 is used. However the stiffness parameters are not taken from the grain material, but are scaled down in order to improve numerical stability by an approach described in [7]. Nonlinear cohesion forces are available in the framework, but are not used for this analysis. In tangential direction the particles are featuring a regularized stick-slip friction model covering the MOHR-COULOMB yield criterion:

$$\vec{F}_\mathrm{T} = \begin{cases} c_\mathrm{T} \cdot \vec{\delta}_\mathrm{T} + k_\mathrm{T} \cdot \dot{\vec{\delta}}_\mathrm{T} & \forall \quad \vec{F}_{c\mathrm{T}} \leq F_\mathrm{N} \cdot \tan(\phi_\mathrm{h}) \\ \vec{F}_\mathrm{N} \cdot \tan(\phi_\mathrm{g}) & \forall \quad \vec{F}_{c\mathrm{T}} > F_\mathrm{N} \cdot \tan(\phi_\mathrm{h}) \end{cases} \tag{12}$$

Thereby $\vec{\delta}_\mathrm{T}$, c_T and k_T are the deflection, stiffness and damping coefficient of the regularization spring-damper element. ϕ_h and ϕ_g are the interparticle sticking and sliding friction angle, respectively. Figure 5 shows an overview of the particle interaction model in normal and tangential contact direction. The additional heuristic approach of background damping k_h is used to apply additional dissipation to particles which are currently not in contact.

Grains in real soils are shaped during their formation and continuous wear, leading to arbitrary, possibly non-convex grain shapes. Direct usage of those shapes as particle geometries would lead to multiple interaction points per contact and further complicated contact detection. As this results in less efficient models and as the particles rotational behaviour influences the macroscale shear strength (cf. [14]), LICHTENHELDT & SCHÄFER [6] proposed an anisotropic modeling approach based on rotation geometries. As explained in [6], Figure 6 shows the mapping of the rotation behaviour of angular grains to three dimensional spherical particles by using two

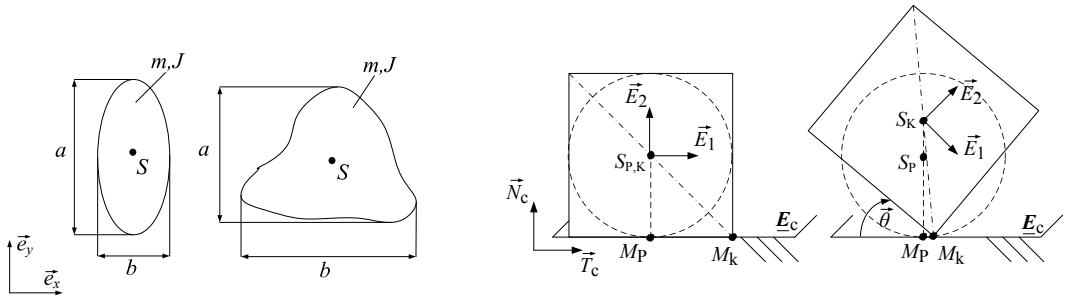

Figure 6: Covering the anisotropic rotational behaviour of angular grains by mapping 2D-rotation geometries to spherical particles [6]

dimensional rotation geometries. These rotation geometries are used to calculate a nonlinear torque based on the tilting motion using normal as well as tangential contact forces. Thereby the rotation geometry can be applied with an aspect ratio $A = \frac{a}{b}$, whereby a and b are the length of the rectangle edges (Fig.6 left). As each rotation degree of freedom of a particle can be assigned with a 2D-rotation geometry, anisotropic rolling behaviour and three dimensional equivalent geometries as shown in Figure 7 are achieved. Each of these 2D-rotation geometries is element of the rotation plane defined perpendicular to the respective rotation axis. Using the total contact force projected in the rotation plane $\vec{F}_{\mathrm{R}}^{jk}$, as well as the projected contact normal and tangential direction vectors $\vec{N}_{\mathrm{c}}^{jk}$ and $\vec{T}_{\mathrm{c}}^{jk}$, the torque $\vec{M}_{\mathrm{RG}}$ is derived as:

$$\begin{aligned} \vec{M}_{\mathrm{RG}} = \sum_{i,j,k=1}^{3} \Big(& \vec{F}_{\mathrm{R}}^{jk} \times \left[l_{\mathrm{T}}^{jk} \left(\theta_i(t), \gamma_i\right) \cdot \vec{N}_{\mathrm{c}}^{jk} \right] + \\ & \vec{F}_{\mathrm{R}}^{jk} \times \left[l_{\mathrm{N}}^{jk} \left(\theta_i(t), \gamma_i\right) \cdot \vec{T}_{\mathrm{c}}^{jk} \right] \Big) \\ i, j, k = & [1, 2, 3] \wedge i \neq j \neq k \end{aligned} \tag{13}$$

whereas l_{N}^{jk} and l_{T}^{jk} are the nonlinear moment arms of the rotation geometry for normal and tangential direction respectively. These moment arms depend on the current orientation of the particle with respect to the contact situation, described by the angle $\theta_i(t)$ and the aspect ratio angle $\gamma_i = \arctan(A),$ with $\gamma \in (0; \frac{\pi}{2})$. Thereby the current rotation with respect to the contact situation is derived from each particles' rotation quaternion $\overline{q} \in \mathbb{H}$ and the contact point.
First validation using DLR-RMC's bevameter has been shown in [7], further validation progress has been carried out and will be shown in section 4.1. of this paper. Using these contact models and approaches it is possible to model granular soils for terramechanics applications in a detailed but computationally robust and efficient way.

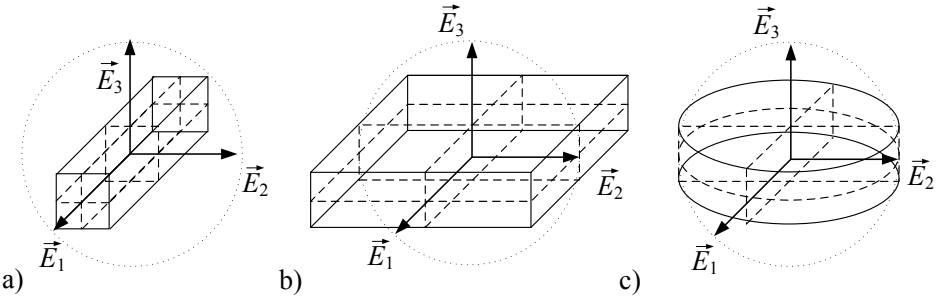

Figure 7: Examples for resulting rotation geometries [6]: a) rectangular bar b) rectangular plate c) cylindrical disc

3.3. HP^3-Mole DEM & Co-Simulation

In order to cover the complex interaction between the hammering mechanism and the soil, a co-simulation coupling the particle-based terramechanics model and the multi-body simulation is set up. Using this approach the mutual interactions and advantages from both domains are directly covered. However, as the HP^3-Mole approaches to a certain depth rather slowly, it is not suitable to perform a DEM-MBS co-simulation all the way down. Thus sequential simulations as shown in Figure 8 are carried out in order to perform one co-simulation stroke in a certain depth. Therefore a domain containing an arbitrary volume of a multitude of parti-

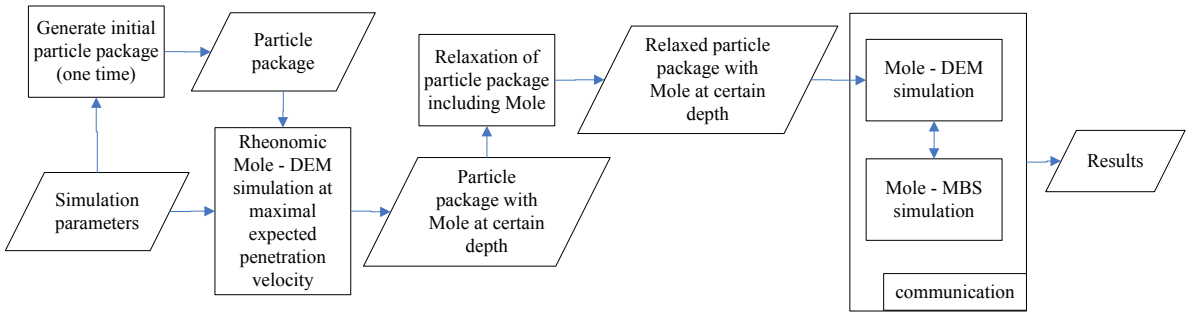

Figure 8: Sequential simulation process to perform the co-simulation

cles, called the particle package hereafter, of $1.4\,\mathrm{m}$ depth is created once and used throughout all simulations. Afterwards the triangularized surface representations of the Mole's outer hull variants are pushed into the soil rheonomically up to a tip depth of $1\,\mathrm{m}$. This depth is chosen as a compromise between calculation time and soil pressure acting on the Mole. It is assumed that this depth is already suitable to perform co-simulations and comparisons between different outer hull variants. The fixed pushing speed is chosen by the expected maximum penetration speed during the stroke cycle of the current Mole design. This velocity has been chosen in order to use the results not only to create a particle package including the Mole in a certain depth, but also to obtain the soil resistance exerted by the different shapes in a soil state similar to the one during the stroke cycle.

In a next step to obtain a suitable particle package for the co-simulation, the particles need to be relaxed. This relaxation is needed, as the simulation stops when the Mole is still driven rheonomically. In real operation there is a time span of more than $3\,\mathrm{s}$ between two subsequent stroke cycles and thus enough time for the soil to relax. Starting with a preloaded package would result in non-realistic upwards motion as the soil would start relaxing during the co-simulation. In order to allow this relaxation to take place, the outer hull is fixed in space and only the particles are allowed to move. As a compromise between computation time and the demand for a relaxed soil, $0.5\,\mathrm{s}$ is chosen as simulation time for this step. This results in computation times of less than one day for the relaxation.

Thereafter the actual co-simulation takes place and is moderated via Matlab-Simulink®, connecting to SIMPACK's and Pasimodo's built-in co-simulation interfaces. In order to be computationally efficient and gather impact loads in the mechanism, the maximum time step for the multi-body simulation is chosen at least one order of magnitude lower than in the particle simulation. The communication step size is chosen equal to the maximum particle simulation time step size.

To keep the computation time as low as possible, dynamic simulation domain boundaries are used that follow the focused body at discrete time steps. Thereby the boundaries of the simulation domain are spatially fixed particles. As the Mole penetrates into the soil particles are loaded and freed beneath the outer hull. Similarly particles above it are fixed and later on

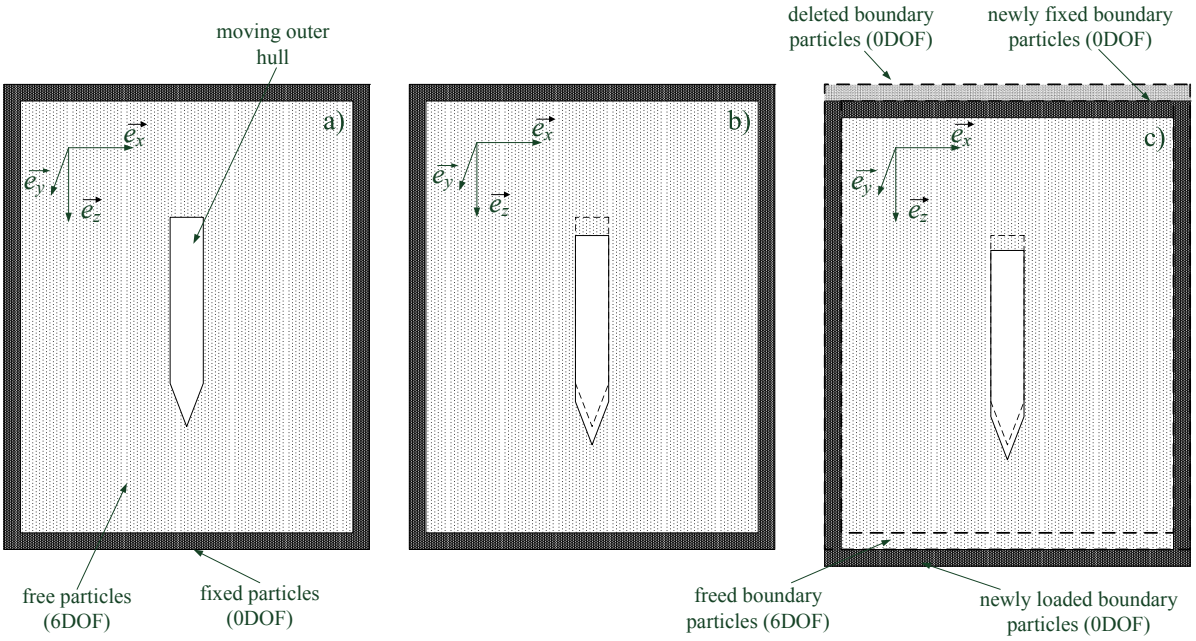

Figure 9: Principle of the dynamic boundary strategy for the Mole DEM simulations

deleted. OBERMAYR et al. [15] originally proposed such an approach based on the tool velocity. For Mole and planetary rover wheel simulations this approach has been enhanced in order to handle dynamic boundaries based on the current position of the tool. Figure 9 exemplifies this approach for the Mole in one direction. In frame a) the initial situation is shown. While the hull is moved in frame b), the loading time step is not yet met and thus the dynamic boundaries are not displaced yet. As the Mole moves further and the trigger time for loading is met, an amount of particles based on the displacement from frame a) to frame c) is loaded, fixed and their kinetic energy is removed. A predefined domain of particles around the Mole is set to 6DOF and all other particles stay fixed as boundary particles. Afterwards the same amount of particles, that has been loaded beneath the Mole is deleted above. Thus a constant, minimum number of particles is used in a limited domain while the overburden pressure in the current depth is conserved. As exemplified in one dimension, this approach is available in all three dimensions. The required DEM interaction parameters for the Mole-DEM simulations are ob-

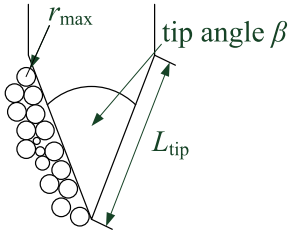

Figure 10: Resolution and tip angle for the Mole's outer hull

tained using the strategy proposed by LICHTENHELDT & SCHÄFER [7]. They are derived for a quartz sand available for tests in the 5 m testbed at DLR Institute of Space Systems (DLR-RY) in Bremen. The aspect ratios and thus the equivalent 3D rotation shape have been set using microscopic pictures of the grains provided by DLR-RY. In order to scale the particle size, a resolution $\Gamma \geq 4$ is used. For the Mole this resolution is defined as:

$$\Gamma = \frac{L_{\text{tip}}}{2r_{\max}} \tag{14}$$

where L_{tip} is the mantle length of the tip and $r_{\max}$ is the maximum particle radius, as shown in Figure 10. For comparability of the simulations the same particle bin is used for the analysis

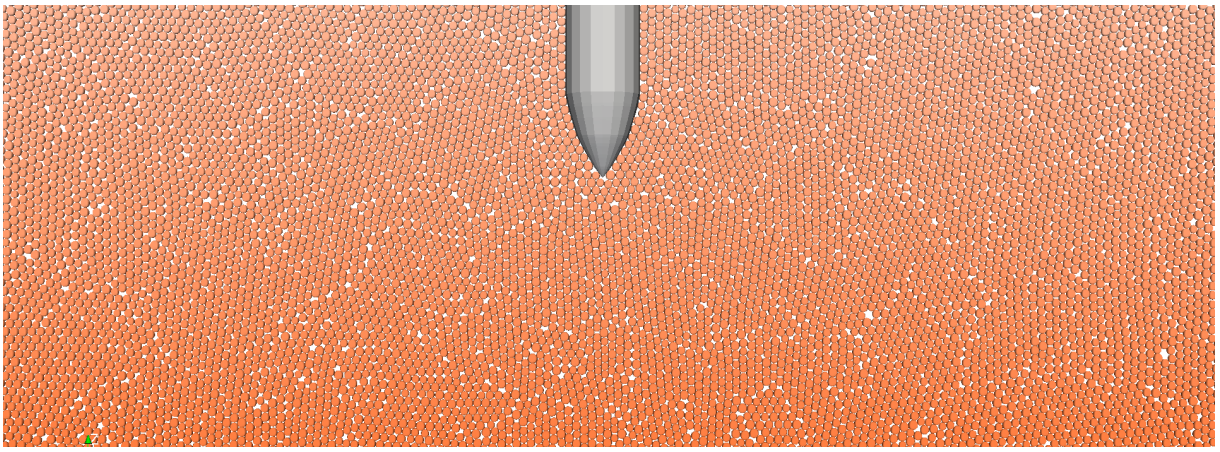

Figure 11: Visualization of part of the prepared particle package for the co-simulation

and additional variations, thus the particle size is scaled for the minimum tip mantle length. This results in a resolution $\Gamma \in [9, 11]$ for the current nonlinear tip. The visualized initial state of the package for the co-simulation is shown in Figure 11. The particles are displayed by their contact representative spherical geometry. The mapped rotation geometry considered for torque computation is not shown in the image. A slight particle size distribution is applied in order to suppress clustering in face centered cubic structures. The factor between the biggest and the smallest particles' radii is 1.25.
Different shapes of the Mole's outer hull can be created based as parametrized surface meshes, as the framework enables automatic creation of suitable surfaces. Using the DEM modeling strategy for the soil, the macroscale soil deformation and effects like plasticity and soil flow are directly covered by the microscale particle displacement. Hence observed macroscale effects can be related to their microscale origin and enable further understanding of the effects in interaction with the soil.

4. RESULTS

The models explained throughout the last sections are used in order to analyze and to enhance the system's performance. Thus the operational cycle of the mechanism has been investigated in detail using the co-simulation approach. With these simulations the coupled model can be compared to deep penetration tests in the laboratory. For all simulations and tests in soil, dry quartz sand is used.

4.1. Validation

In order to investigate the accuracy of the different simulation modules, validation of the models has been carried out in several steps. In the first stage the enhanced multi-body model of the hammering mechanism has been compared to measurements of prototypes. To enable high accuracy in the measurements as well as to disable influences from the soil, the validation of the mechanism model is carried out on the Mole's Health Check Teststand (HCTS). As shown in Figure 12 (right), on this device the Mole is acting against a spring and guided radially. The spring deflection is measured by a laser sensor and stored with sufficiently high resolution in time. The development of the device as well as the measurements were performed at DLR Institute of Space Systems in Bremen. Similar to the validation of models of older Mole prototypes shown in [4], measurements are taken for 100 nominal strokes and the time dependent mean as well as the standard deviation are calculated from the measured data. Using the mean $\overline{\delta}_{z\mathrm{m}}(t)$

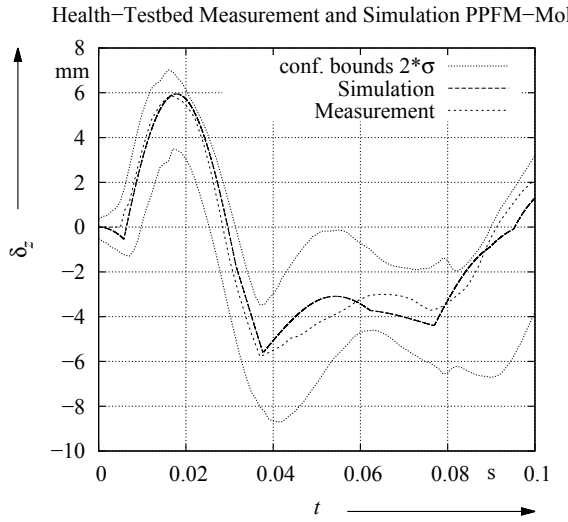

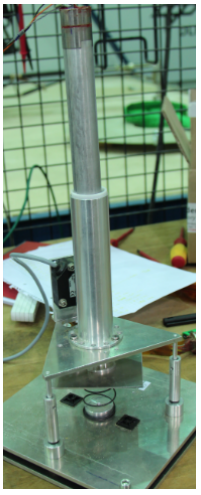

Figure 12: Comparison of measurement and simulation on the HCTS (left) and picture of the Mole on the HCTS (right)

and the standard deviation σ, the time dependent confidence intervals $\varsigma(t)$ can be retrieved as:

$$\varsigma(t) = \overline{\delta}_{z\mathrm{m}}(t) \pm 2 \cdot \sigma(t) \tag{15}$$

Confidence intervals for 2σ are used to cover 95.4% of the measured values. Figure 12 left shows the comparison of the measurement of a nominal stroke and the confidence interval to the simulated HCTS test. It can be seen, that good correlation is achieved by the proposed mechanism model. The energy and timing of the first as well as the second and subsequent strokes (cf. section 2., 4.2.) are covered accurately by the model. Remarkably the behaviour after the second stroke (on Earth) can only be covered if the inner gas dynamics model is used. Using an older viscous element approach, the behaviour differs from the measured trajectory, as the simulated mechanism does not show sufficiently high energy at the second stroke. This is assumed to be caused by an additional stiffness introduced by the enclosed gas. These effects are of lower influence in Martian environment. In addition to the HCTS tests, acceleration measurements on the suppressor have been used to check the simulation results and the timing of the inner effects. Motor current measurements were used to check the correlation to the motor and tensioning model. By evaluating the current in simulation as well as measurement a peak power consumption of less than $5\,\mathrm{W}$ is observed and the simulated current profile shows good correlation with the measured ones. Furthermore high speed camera recordings of the mechanism in a non-moveable transparent hull were used to check the qualitative behaviour. All of the additional tests showed good correlation with the simulated data, too.
In order to validate the discrete element soil model for the Mole, a simulation for the cone penetrometer test in the freshly prepared $5\,\mathrm{m}$ testbed (DLR-RY) was carried out. The penetrometer tests have been performed in several different radial positions in the testbed up to the full depth. Similar to the approach used in Eq.15, the confidence intervals for 95.4% of the measured values are computed by the depth dependent mean and standard deviation. It needs to be mentioned that most measured points below the mean are already contained within 1σ, whereas few measured points are only outside the upper confidence bound. In addition an individual measurement is shown in Figure 13 left. The simulation is carried out similar to the Mole pushing simulation (section 3.3.). Thus the same initial particle package is used together with the interaction parameters obtained for the quartz sand in the previous section. In order to get the tip resistance stress σ_{tip}, the frictional stress is subtracted from the total resistance stress. In the first $0.1\,\mathrm{m}$ depth, the simulated tip stress is above the measurement values and slightly outside of the

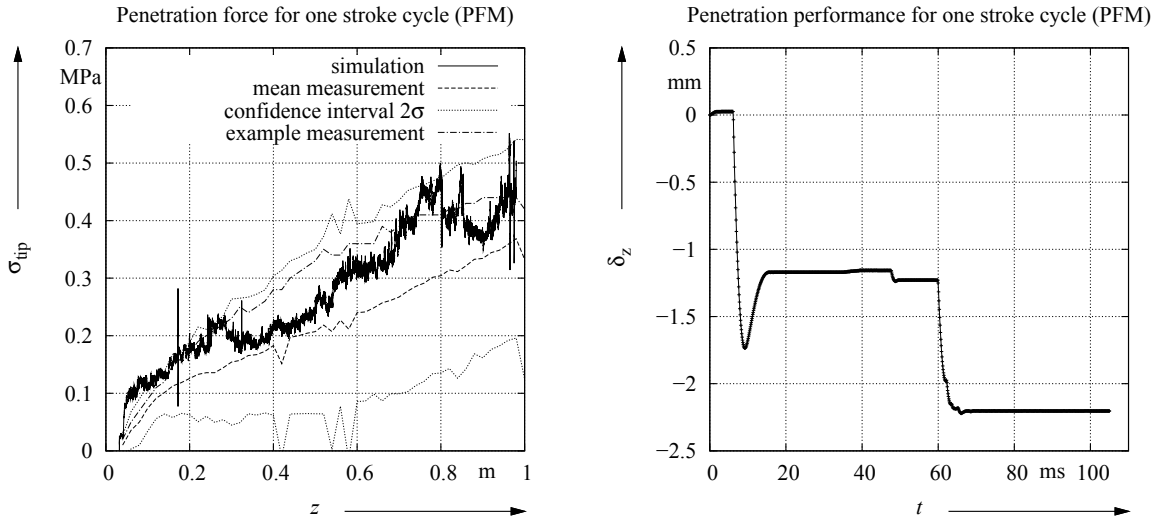

Figure 13: Comparison of the penetrometer measurement and the respective DEM simulation (left) and penetration depth for one stroke cycle of the Mole co-simulation (right)

confidence bounds, which might be caused by the radially restricted simulation domain and a slight relaxation of the particle package. As the device is proceeding further into the package, the simulated results are contained in the confidence intervals with a declining tendency towards the mean. Between 0.1 m to 0.8 m the tip resistance is rising again. The deviations in the simulation results are not present in the real measurements and are caused by the discretisation of the domain, since the particles are bigger than the real grains. Generally the simulated resistance is higher than the mean of the measurements, but still contained within the confidence bounds. As deeper parts of the soil as well as higher tip resistance in general are more challenging for the Mole, the particle package and parameters are suitable to conduct simulations and variations for the Mole.

Additionally a full stroke has been simulated in a depth of 1 m using the current Mole mechanism and outer shape. Figure 13 right shows the penetration depth for this stroke. The achieved penetration of 2.2 mm is in good agreement with the mean penetration of 1.8 mm in the same depth range of the real deep penetration measurement. Furthermore the penetration trajectory covers both, the significant strokes as well as the expected rebound due to the elastic soil behaviour after the first stroke. After the second impact almost no elastic rebound is visible. This effect occurs due to the subsequent strokes which still have sufficiently high energy to cancel out the soil reflow. The displacement is shown in the mechanism's coordinates, with $\vec{E}_z$ pointing upwards.

4.2. Operational Cycle of the Protoflight Mole

As the MBS-DEM co-simulation enables to cover the interaction between mechanism and soil dynamics, the operational cycle of the mechanism can be observed by simulation. Figure 15 shows the velocity profile of the three main bodies of the MBS model with respect to the mechanisms coordinate system. The operational cycle of the stroke process starts, after tensioning is completed, in the state shown in Figure 14 frame 1. The hammer as well as the suppressor are accelerated by the springs, as the roller releases the cam. The hammer separates from the force springs at their initial length, moving freely towards the tip. Right after reaching its maximum velocity the hammer impacts the outer hull at the tip (Fig.14 frame 2 and Fig.15 I) and the hull starts to penetrate the soil. After the impact the hammer slightly rebounds from the tip. While the impact takes place, the suppressor is still moving upwards, decelerated by the brake spring, friction and the inner gas flow (Figure 14 frame 3). After the maximum allowed distance be-

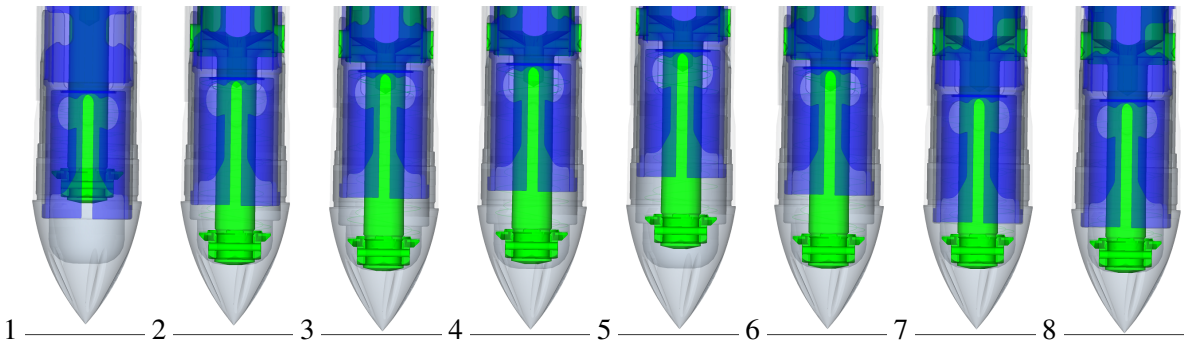

Figure 14: Animation of the operational cycle of the HP^3-Mole derived by co-simulation

tween hammer and suppressor is met (Figure 14 frame 4 and Figure 15 II), a mechanical stop closes and the hammer is taken upwards with the suppressor while they are still moving in different directions. However due to the lower relative velocities the contact causes significantly lower loads compared to former results of an earlier prototype presented in [4]. Because of the impact the hammer gets faster than the suppressor. In Figure 14 frame 5 the suppressor reaches its point of reversal, due to the brake spring. As the suppressor is moving downwards together with the hammer, the latter is still separated from the force springs. Thus the following impact of the hammer at the tip in Figure 14 frame 6 (Figure 15 III) has only limited impact energy, as the suppressor is not coupled to the hammer yet. In the next frame and at point IV in Figure 15, the suppressor impacts the tip and causes the second stroke (frame 7), resulting in significant penetrating motion of the outer hull. Before the Mole is totally stopped by the resistive soil force, the subsequent third stroke occurs in point V, leading to a prolonged penetration motion and a cancellation of the soil reflow. Thus after the second and third stroke almost no macroscopic elastic rebound of the outer hull is visible. Due to the inertial and gravitational forces, the hammer is accelerating in negative $\vec{E}_z$ direction after the outer hull is displaced in point IV. After the Mole is finally stopped by the outer forces, the hammer impacts the tip again in point VI. Due to the low energy of the hammer, the penetration efficiency of this impact is negligible. Similarly subsequent strokes of the suppressor follow point V, which are insignificant for the locomotion as well. The Mole rests in its initial position again in frame 8 until the roller reengages the cylindrical and starts the tensioning process anew.
While the inner processes in the mechanism take place the soil is subject to shock loads at each inner impact. As the particles are connected by contacts the hammering mechanism causes

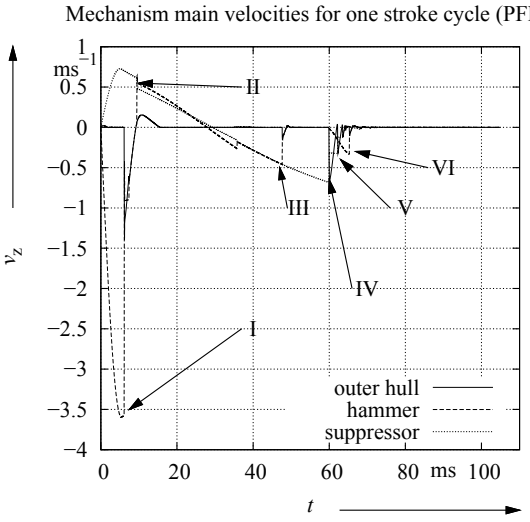

Figure 15: Velocity profile for the main bodies derived by co-simulation

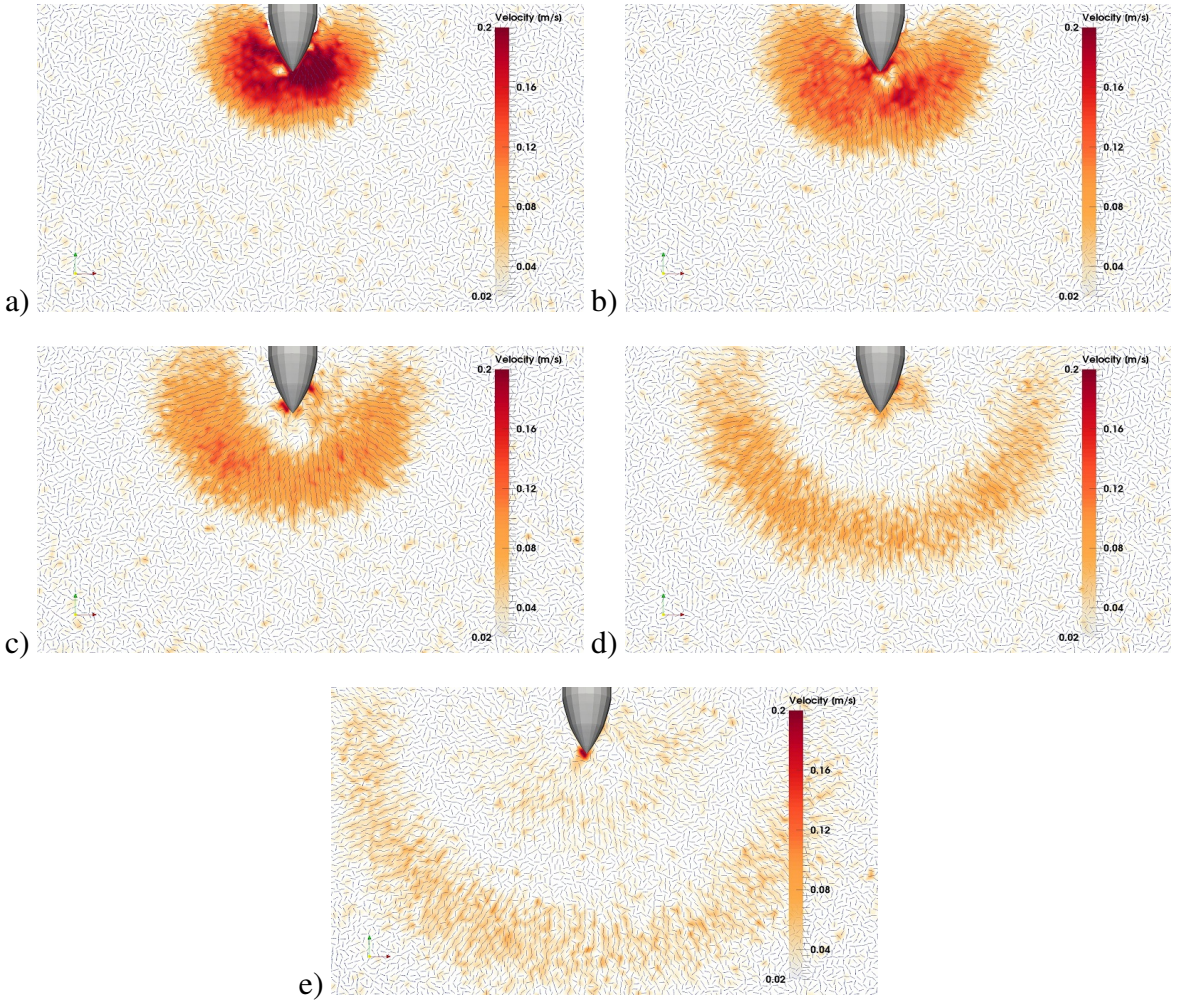

Figure 16: Animation of the shock wave induced by the operation of the HP^3-Mole: First stroke

shock waves traveling through the soil. Figure 16 shows the shock wave profile of the first stroke at different times. The domain is colored by the interpolated absolute velocity and bars showing the particle movement are attached to the individual particles. Colored areas not influenced by the shock wave are caused by local relocation of particles due to voids in the virtual soil and the overburden pressure. Frame a) is taken 2.5 ms after the impact, whereas b) and c) each are taken in sequence with 1 ms delay. Next to the tip, the soil reflow starts to build up. In frame d) 2 ms later, the intensity of the wave and the particle velocity are already lowered remarkably. Additional 3 ms later the reflow is almost extinct again in frame e).
Figure 17 shows the second, shortly followed by the third stroke (point IV and V in Fig.15). Frame 1 is taken 1.5 ms after the second stroke. All subsequent frames are taken with a delay of 1 ms. The second stroke itself is weaker and causes lower particle velocities inside the shock wave. For the second/third stroke it is remarkably, that no noticeable soil reflow is building up. The constant darker red spot right at the tip is caused by the discrete nature of the particles interacting with the sharp edge of the tip causing local vibrations. Using these observations for the second/third stroke, it can be assumed that the subsequent third stroke occurs just in time to extinguish the soil reflow wave.
This effect should be subject to further research in order to determine if the shock waves are covered sufficiently by the simulation to use them as criteria for design decisions. Furthermore it shall be checked if the effect can be used in order to improve locomotion performance and efficiency by lowering the macroscopic rebound motion due to soil reflow.

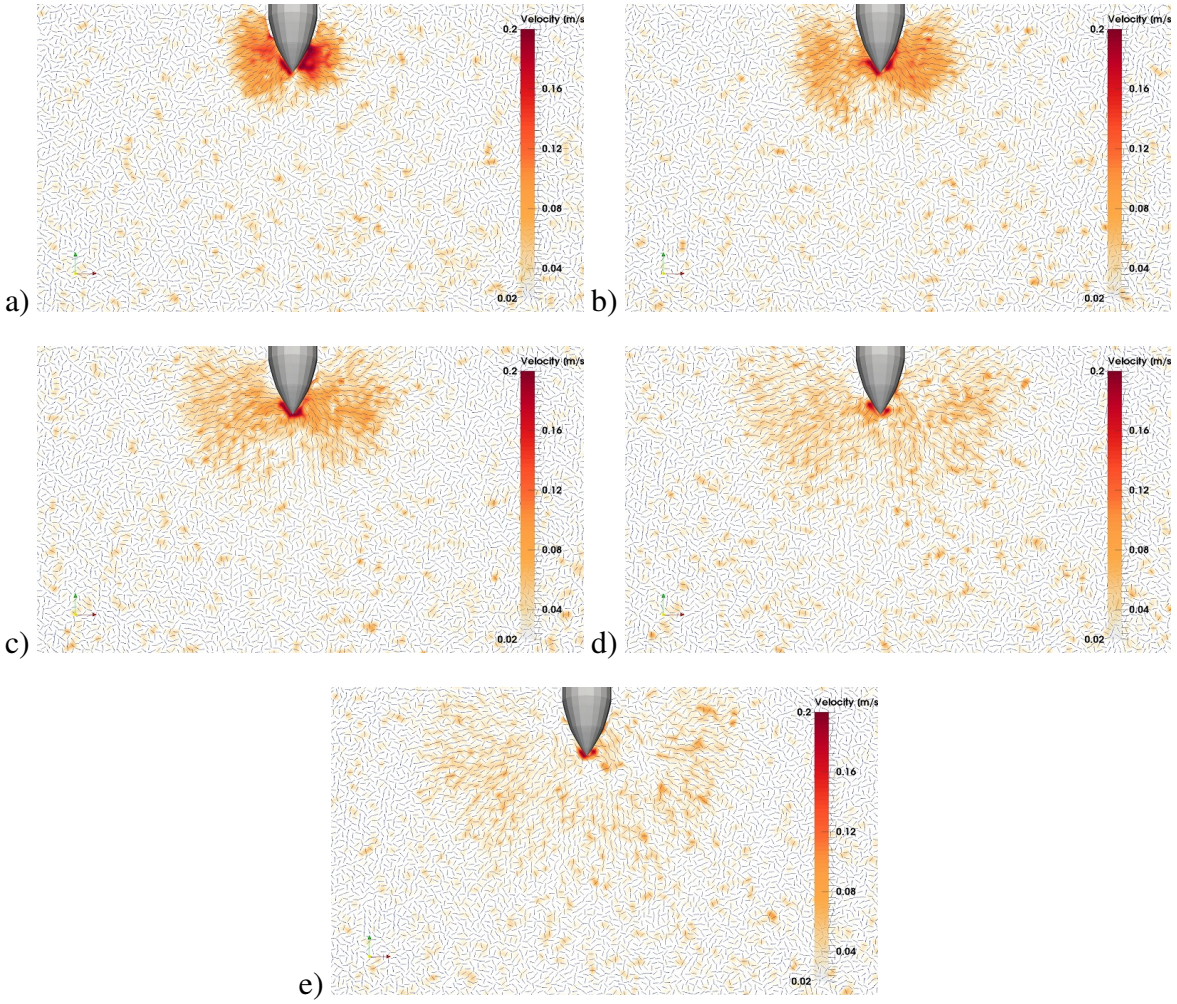

Figure 17: Animation of the shock wave induced by the operation of the HP^3-Mole: Second stroke

5. CONCLUSION

Since prior test campaigns in actual Martian environment are not possible, high fidelity simulation models for InSight's HP^3-Mole are required. By applying a co-simulation approach between an enhanced multi-body dynamics model and a particle-based soil model, the demand for high accuracy and independence of preliminary calibration is met.

Therefore the mechanism model covers the full tensioning process including the DC-motor dynamics and the stroke cycle including internal contact dynamics. Good correlation for both, mechanism and soil model has been achieved. By comparing the current inner air flow model to an older viscous force model, it could be shown, that it is not possible to cover the full stroke cycle in simulation without detailed modeling of the inner gas flow. Furthermore the gas flow model enables the coverage of the effects by known environmental parameters without the need of calibration.

In order to cover the soil behaviour a DEM model and parameter estimation strategy, originally developed for planetary rover wheels, are adapted to the Mole. This model is able to cover the soil deformation effects induced by the impact driven locomotion on macroscale as it explicitly covers the particle displacement on microscale. Using a rotation geometry mapping to determine the particle torques, spherical particles can be used as contact bodies while still covering the rotational behaviour of arbitrarily shaped grains. Additionally by applying dynamic boundaries a constant minimum size of the simulation domain is achieved while maintaining

the overburden pressure.
Nevertheless the co-simulation is time consuming as it needs several preparation simulations in order to obtain a particle package containing the Mole in a certain depth. Additionally in order to precisely model the soil a certain resolution and corresponding particle size is needed causing a high number of contacts which results in long simulation times. Thus for longer lasting operation simpler models like elasto-plastic elements should be used and calibrated by the co-simulation or real tests. Furthermore the propagation of the shock wave inside the soil should be further analyzed and compared to measurements in later work. Due to the decreasing particle velocities it is presumed that the waves are traveling with non constant speed and are thus supposed to be nonlinear wave propagation phenomena. The shock wave profile and propagation could also be used in order to optimize the inner mechanism timing as well as the outer shape.
Summarizing, a modeling approach to cover the impact driven locomotion of the Mole was presented and proved to satisfactorily predict the Mole dynamics. Hence ongoing work will focus on usage of this model in order to analyze the current system, as well as to develop and optimize future Mole systems. E.g. intermediate results of the co-simulation can be used to determine further influences: Mole pushing simulations for different tip shapes will be used in order to compare resistive soil forces exerted by the outer shape. Furthermore the influence of the soil on the tip shape to resistance force relation is a task of scientific interest.

REFERENCES

[1] NASA InSight Homepage: http://insight.jpl.nasa.gov, checked 12/2013, NASA, 2013

[2] Lichtenheldt, R.; Schäfer, B.: Hammering beneath the Surface of Mars - Modellbildung und Optimierung des HP3-Mole, In L. Zentner (Ed.) Proceedings of "10. Kolloquium Getriebetechnik", pp. 169-186, ISBN 978-3-86360-065-5, Ilmenau, Germany, 2013

[3] Joos, H.-D.; Bals, J.; Looye, G.; Schnepper, K.; Varga, A: A multi-objective optimisation-based software environment for control systems design, IEEE International Conference on Control Applications and International Symposium on Computer Aided Control Systems Design, Glasgow, Scotland, UK, pp. 7-14, 2002

[4] Lichtenheldt, R.; Schäfer, B.; Krömer, O.; van Zoest, T.: Hammering beneath the Surface of Mars - Forensic Engineering of failures in the HP^3-Mole by applying multi-body dynamics simulation, Proceedings of 3rd International Conference on Multibody System Dynamics IMSD 2014, ISBN 978-89-950027-7-3, Busan, Korea, 2014.

[5] Grygorczuk, J.; Seweryn, K.; Wawrzaszek, R.; Banaszkiewicz M.: Technological features in the new mole penetrator "KRET", ESMATS: 13th European Space Mechanisms And Tribology Symposium, Vienna, Austria, 2009

[6] Lichtenheldt, R.; Schäfer B.: Planetary Rover Locomotion on soft granular Soils - Efficient Adaption of the rolling Behaviour of nonspherical Grains for Discrete Element Simulations, 3rd International Conference on Particle-Based Methods, pp. 807-818, ISBN 978-84-941531-8-1, Stuttgart, Germany, 2013

[7] Lichtenheldt, R.; Schäfer, B.: Locomotion on soft granular Soils: A Discrete Element based Approach for Simulations in Planetary Exploration, 12th Symposium on Advanced Space Technologies in Robotics and Automation, ESA/ESTEC, Netherlands, 2013

[8] Iwashita, K.; Oda, M.: Mechanics of Granular Materials: An Introduction, Balkema, Rotterdam, Netherlands, p. 356, 1999

[9] Böswirth, L.: Technische Strömungslehre, pp. 291-302, ISBN 978-3-8348-0272-9, Vieweg & Sohn Verlag, Wiesbaden, Germany, 2007

[10] Süße, R. (Ed.); Diemar, U.; Kallenbach, E.; Marx, B.; Ströhla, T.: Theoretische Grundlagen der Elektrotechnik 2, first edition, p. 558, Teubner/Springer, Wiesbaden, Germany, 2006.

[11] Pinna, S. et.al.: Investigation of the dynamical behaviour of the penetrometer "Mole" by accelerometry: A procedure for the correct integration of shock acceleration data, Prof. Intern. Workshop on Penetrometry in the Solar System, Graz, Verlag der Österreichischen Akademie der Wissenschaften, Austria, 1999

[12] Cundall, P. A.; Strack, O. D. L.: A discrete numerical model for granular assemblies, Geotechnique, Volume 29, Issue 1, pp. 47-65, 1979

[13] Fleissner, F.: Pasimodo v1.12.3: software package and template files, Inpartik & ITM University of Stuttgart, Tübingen/Stuttgart, 2013

[14] Oda, M.; Iwashita, K.: Study on couple stress and shear band development in granular media based on numerical simulation analyses, International Journal of Engineering Science, Volume 38, Issue 15, pp. 1713-1740, 2000

[15] Obermayr, M.; Vrettos, C.; Eberhard, P.: A Discrete Element Model for Cohesive Soil, 3rd International Conference on Particle-Based Methods, pp. 783-794, ISBN 978-84-941531-8-1, Stuttgart, Germany, 2013

CONTACTS

Roy Lichtenheldt, M.Sc. Roy.Lichtenheldt@[dlr.de, tu-ilmenau.de]
Dr. Bernd Schäfer Bernd.Schaefer@dlr.de
Dipl.-Ing.(FH) Olaf Krömer Olaf.Kroemer@dlr.de